Supplementary Information

Light-driven cation pumping in atomic-level cascaded van der Waals heterostructures towards efficient osmotic energy harvesting

Yifan Guo,[a,b] Xi Wang,[a,b] Xinyu Chen,[a,b] Xinyue Cao,[a,b] Zhengwei Cao,[a,b] Cuiwen Zong,[a,b] Jia Ge,[a,b] Junzhu Tao,[a,b] Yu Zhang,[a,b] Gao Liu,[a,b] Lei Jiang[a,b] and Zhen Zhang*[a,b]

[a]School of Chemistry and Materials Science, University of Science and Technology of China, 230026, Hefei, Anhui, China. E-mail: zhenzhang@ustc.edu.cn

[b]Suzhou Institute for Advanced Research, University of Science and Technology of China, 215123, Suzhou, Jiangsu, China.

Supplementary notes

Structural characterization of GO-COF membrane

The successful formation of GO-COF heterostructure under aqueous conditions was further confirmed by X-ray diffraction (XRD), Fourier-transform infrared spectroscopy (FTIR), and X-ray photoelectron spectroscopy (XPS). Compared with pristine GO, whose characteristic diffraction peak appeared at $2\theta \approx 10°$, the composite exhibited a slight low-angle shift, while a broad diffraction feature between 18° and 25° was assigned to π-π stacking between COF layers, corresponding to the (002) plane (Fig. S3). These features indicate that GO served as an interfacial nucleation scaffold, inducing ordered COF stacking on its surface. FTIR spectra displayed characteristic bands at 1640, 1580, and 1180 cm^{-1}, attributable to C-N bonds, imine (-C=N-) linkages, and O=S=O vibrations, respectively, evidencing effective chemical interactions between COF and GO nanosheets (Fig. S4). Raman spectroscopy further supported this conclusion, with C-N and imine-related peaks observed at ~1390 and ~1590 cm^{-1}, while the GO D band remained discernible, indicating preservation of the graphene oxide framework during chemical modification (Fig. S5). High-resolution XPS O_{1s} spectra revealed contributions from C=O, S=O, and S-O species following COF growth, consistent with the incorporation of sulfonated COF components (Fig. S6).

Stability Test

The membrane was fixed in the electrochemical cell and continuously immersed in the electrolyte during the stability test. The external load resistance was kept constant, and the current output was recorded 24 h over seven consecutive days. The power density was calculated from the measured current and resistance. To maintain a stable concentration gradient, the salt solutions were refreshed every 24 h, and the cell was rinsed before each measurement to ensure consistent testing conditions.

Supplementary figures

Fig. S1. Photograph of GO-COF nanosheets, showing a distinct brown-reddish coloration compared with pristine GO.

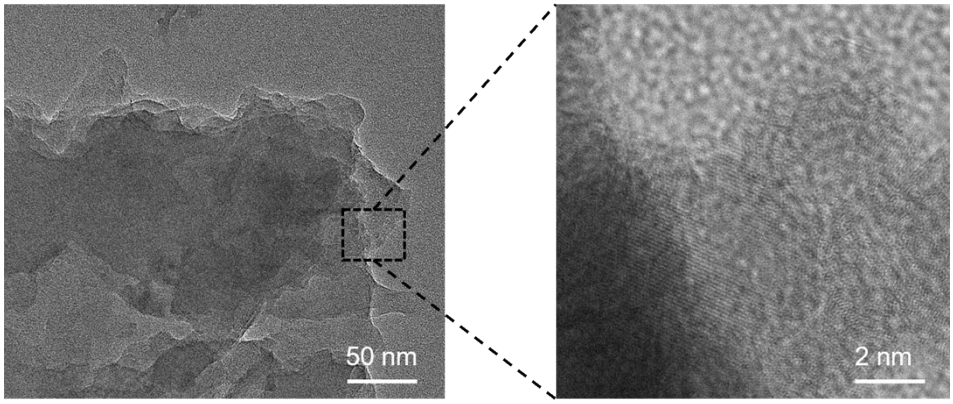

Fig. S2. HRTEM cross-sectional image of the GO-COF nanosheets, revealing the layered stacked structure of the material.

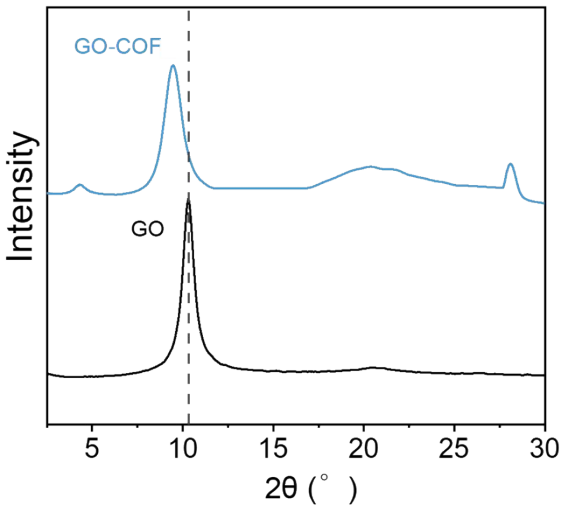

Fig. S3. XRD patterns of GO and GO-COF membrane. The black and blue lines represent the peak positions of GO and GO-COF, respectively.

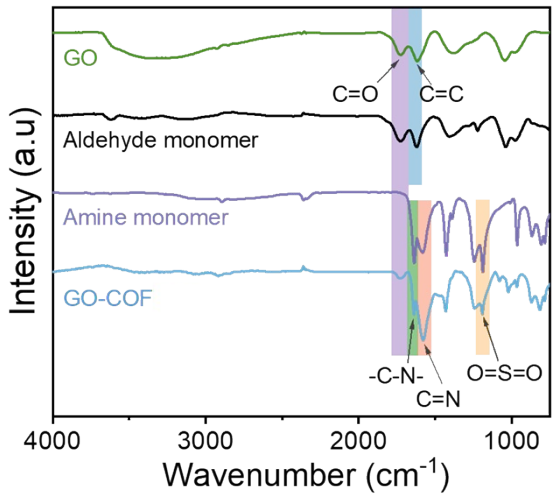

Fig. S4. FTIR spectra of GO membrane, monomers power and GO-COF membrane.

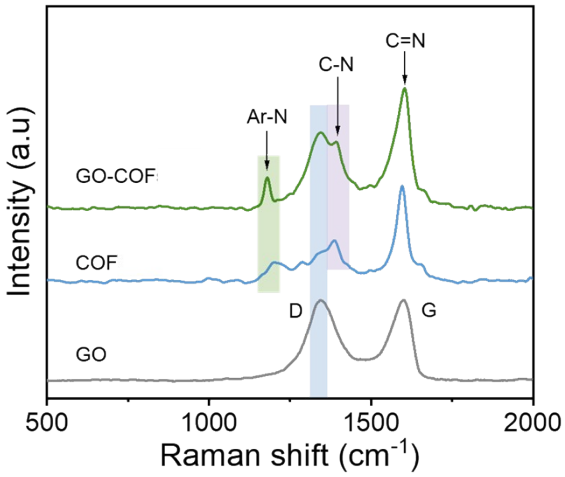

Fig. S5. Raman spectra of GO, COFs and GO-COF membrane.

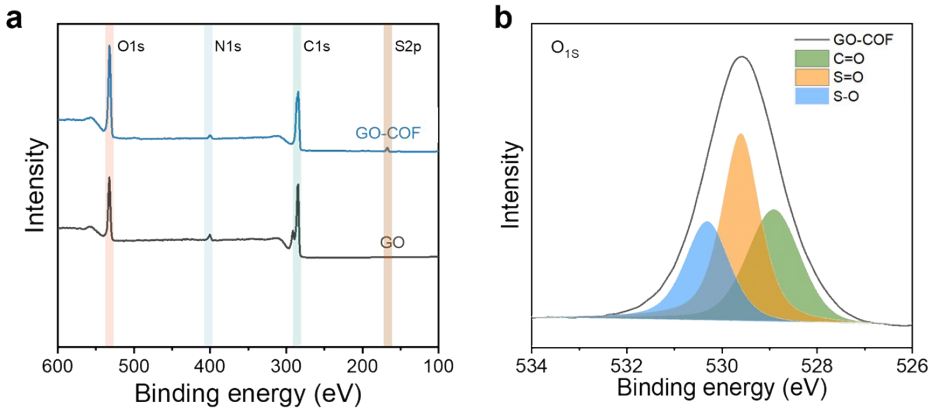

Fig. S6. (a) XPS spectra of GO and GO-COF membrane. (b) High-resolution O_{1s} XPS spectrum of GO-COF membrane.

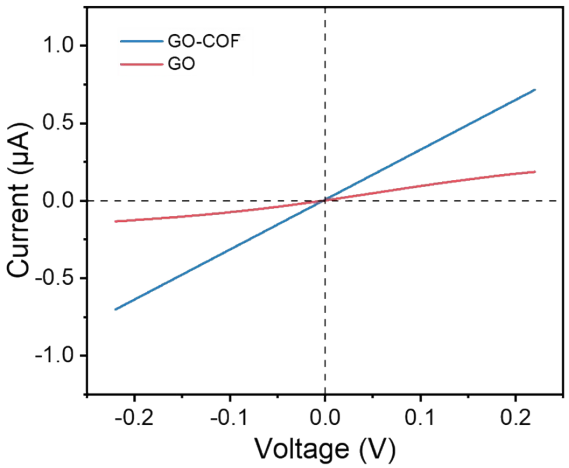

Fig. S7. The *I-V* curves of GO (red) and GO-COF (blue) membranes in 10^{-5} M NaCl solution. The ionic conductance of GO-COF membrane is much higher than GO, indicating the optimized cation transport performance across the GO-COF membrane.

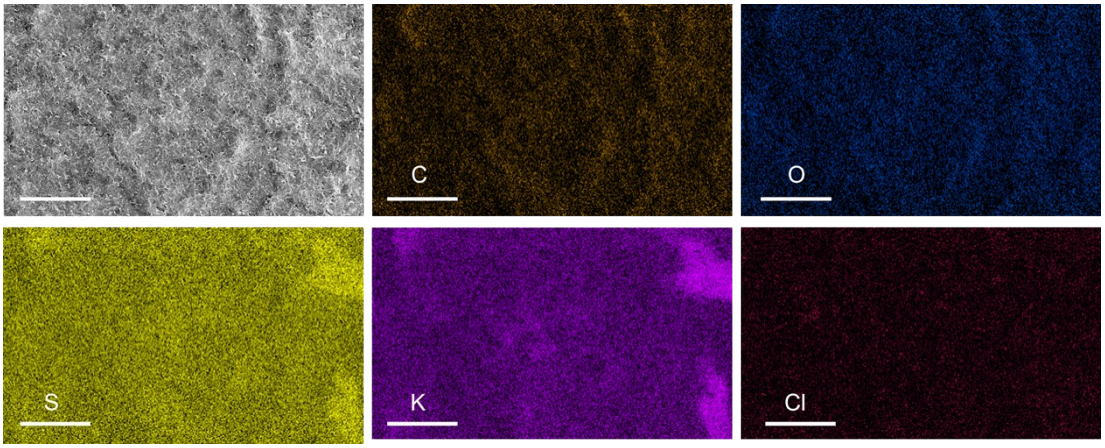

Fig. S8. SEM image and corresponding elemental mappings of the GO-COF membrane after soaking in KCl solution (0.1 M) (Scale bar: 2 μm). K^+ shows a stronger signal than Cl^-, indicating the cation selectivity of the GO-COF membrane.

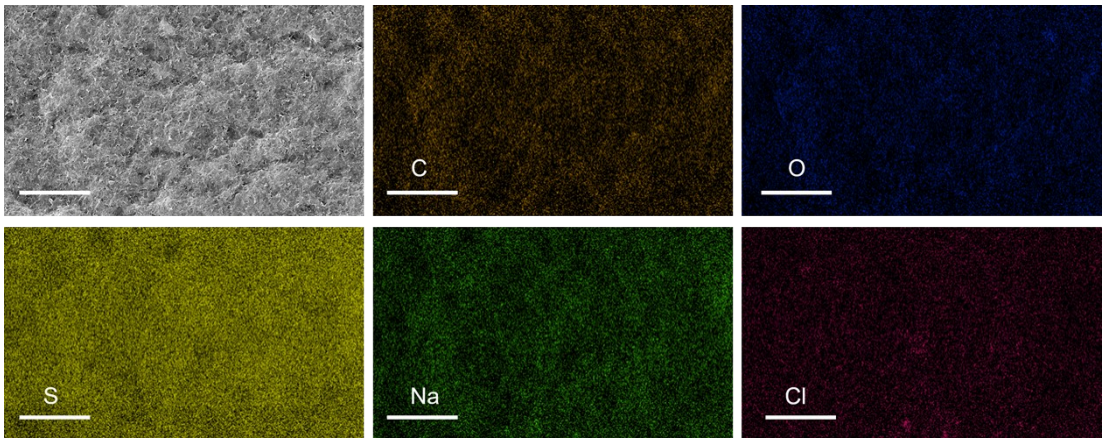

Fig. S9. SEM image and corresponding elemental mappings of the GO-COF membrane after soaking in NaCl solution (0.1 M) (Scale bar: 2 μm). Na^+ shows a stronger signal than Cl^-, indicating the cation selectivity of the GO-COF membrane.

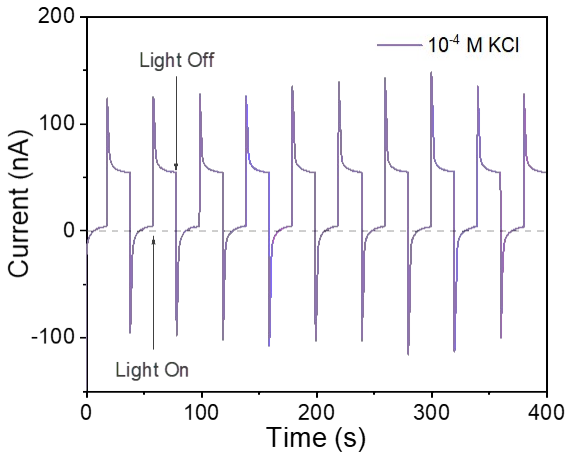

Fig. S10. Light-induced transmembrane ionic current of the GO-COF membrane under zero external bias, demonstrating reversible and directional photo-regulated ion transport.

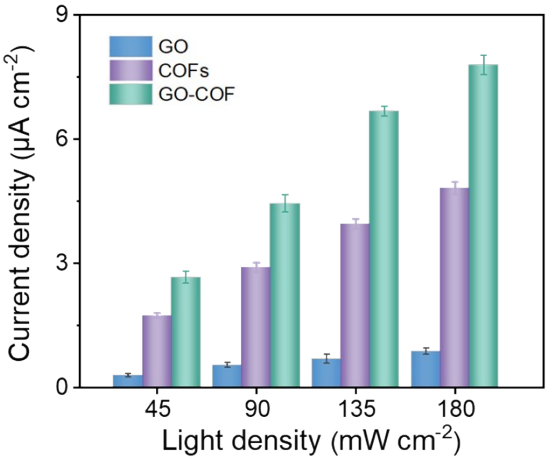

Fig. S11. Photocurrent density of the GO, COFs and GO-COF membrane at different light power densities.

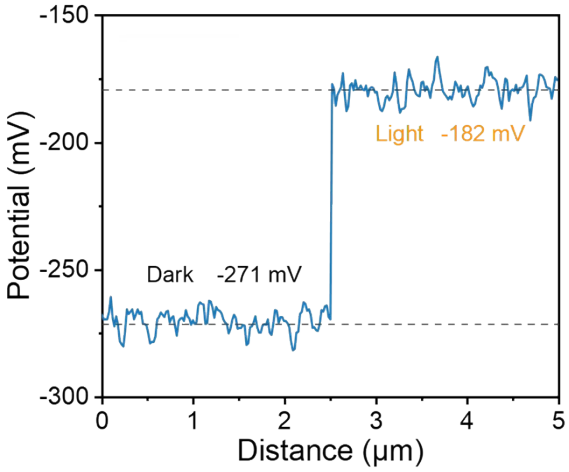

Fig. S12. The surface potential between the sample and Si substrate under light and dark from KPFM measurement.

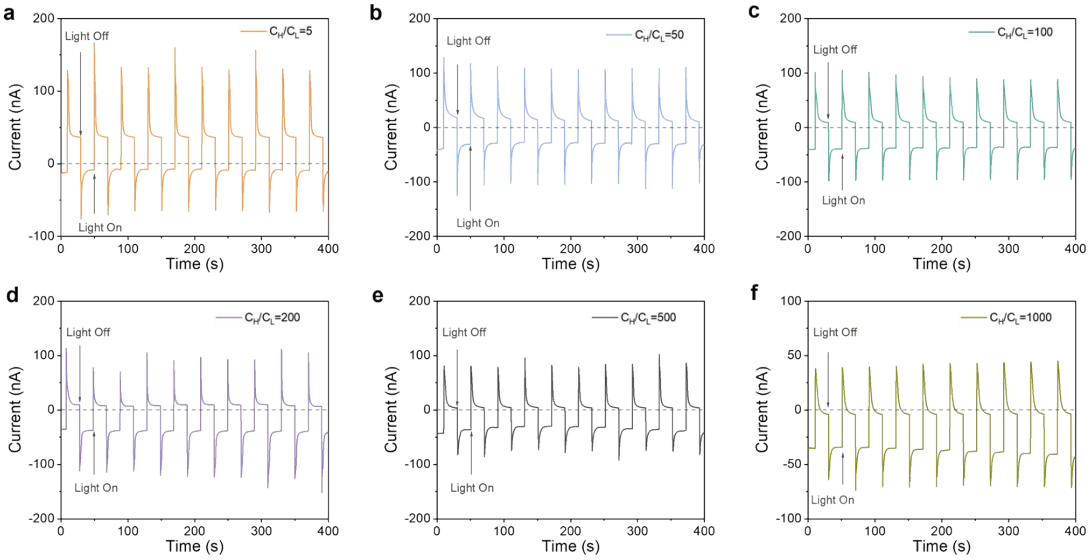

Fig. S13. Time traces of photocurrent under 5-fold to 1000-fold concentration gradient.

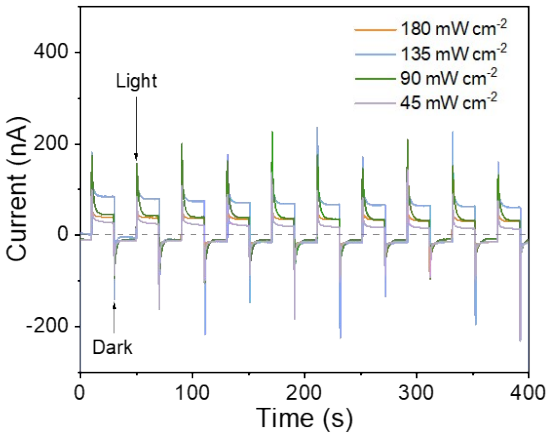

Fig. S14. Photocurrent response dynamics of the GO-COF membrane under varying light densities.

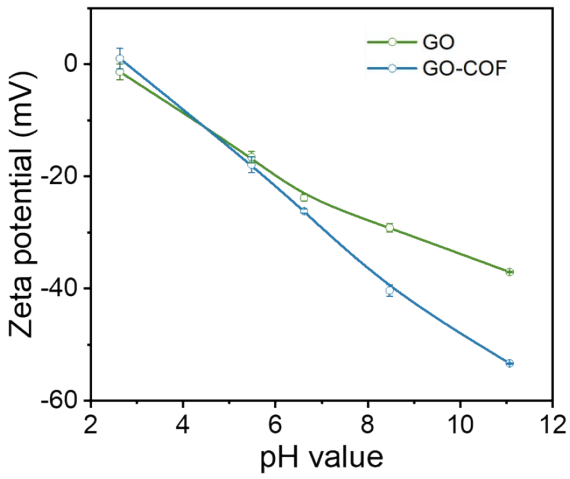

Fig. S15. Zeta potential of GO and GO-COF membrane.

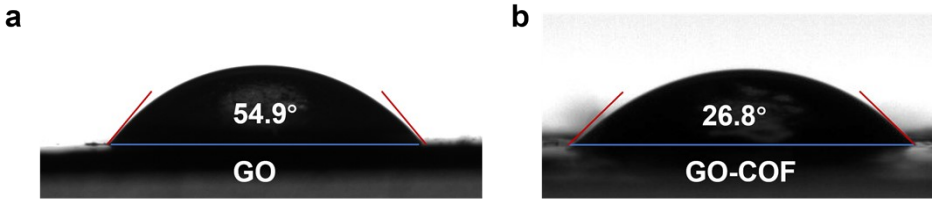

Fig. S16. Contact angle of GO and GO-COF membrane.

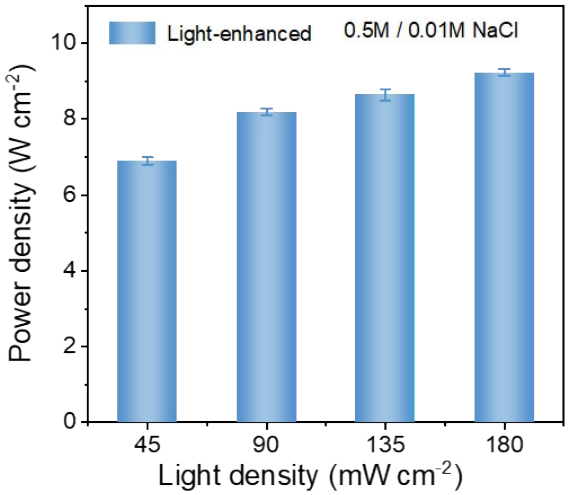

Fig. S17. Light-enhanced osmotic power density under different illumination power densities.

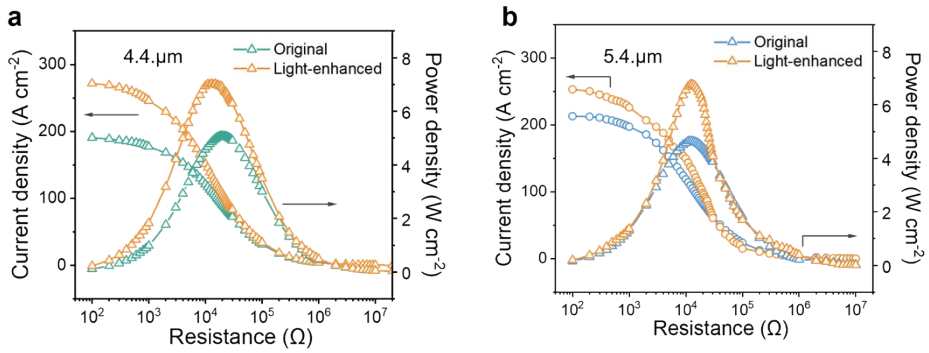

Fig. S18. Thickness-dependent output power density and current density of GO-COF membranes.

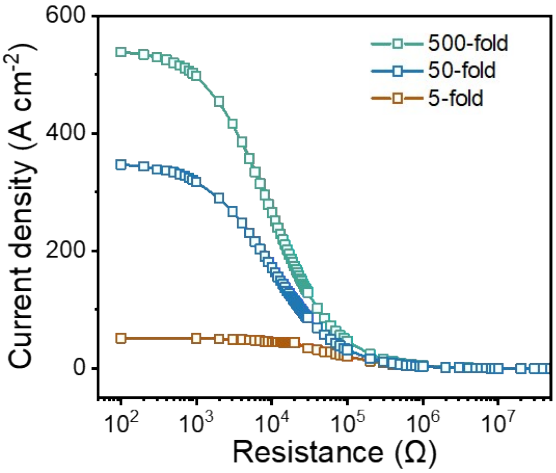

Fig. S19. Current density of GO-COF membrane under different NaCl concentration gradients, with the low-concentration side fixed at 0.01 M.

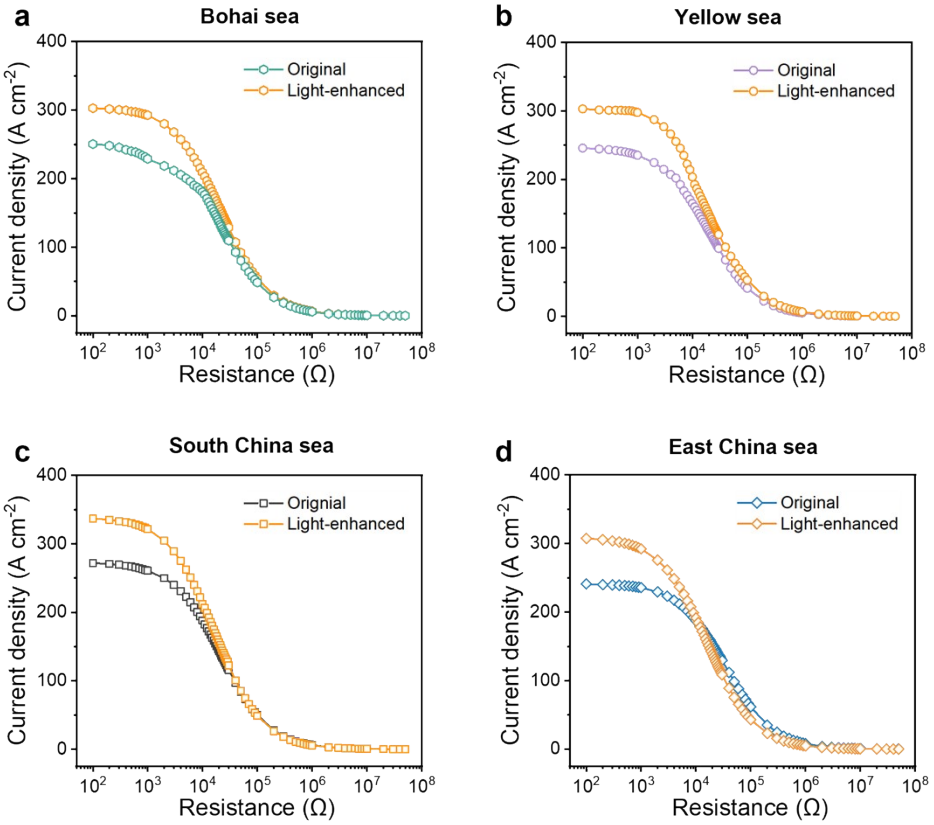

Fig. S20. Current density of GO-COF membranes under real river-seawater conditions.

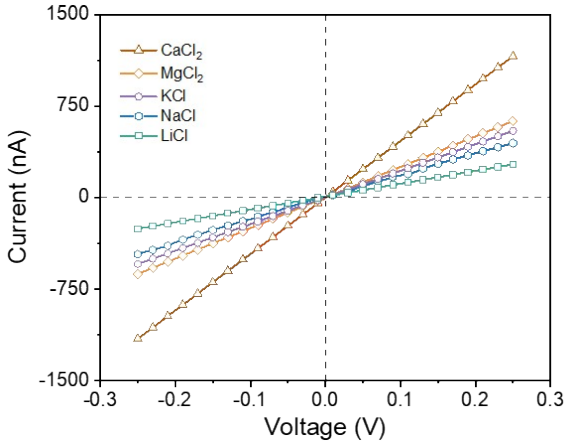

Fig. S21. *I-V* curves of the GO-COF membrane under different types of salt solutions.

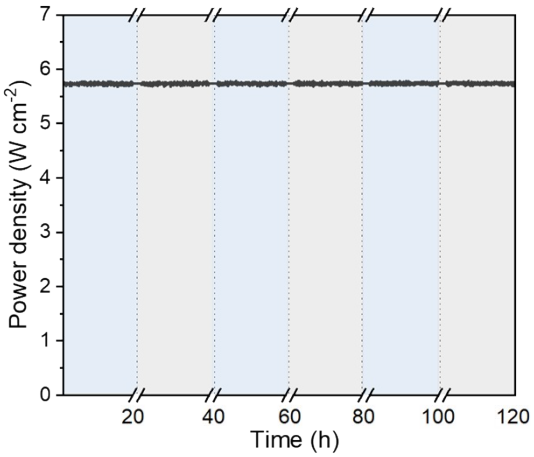

Fig. S22. Long-term stability of the GO-COF membrane under 50-fold concentration gradient.

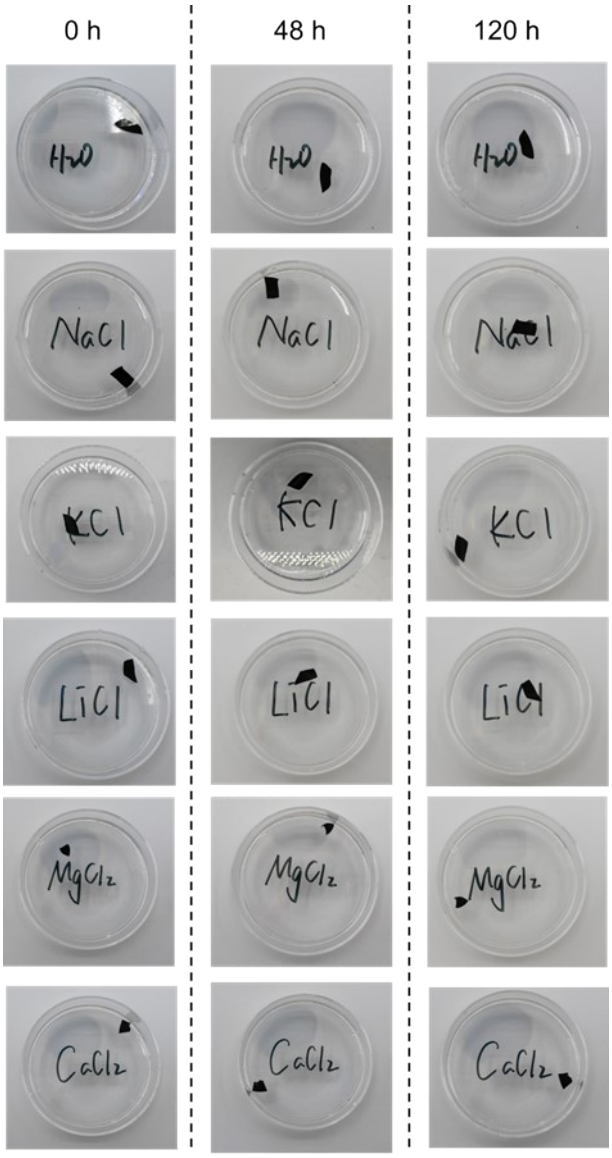

Fig. S23. Photographs of the GO-COF membrane after immersion in different solutions (H_2O, NaCl, KCl, LiCl, $MgCl_2$ and $CaCl_2$; 0.1 M) for 0, 48, and 120 h.

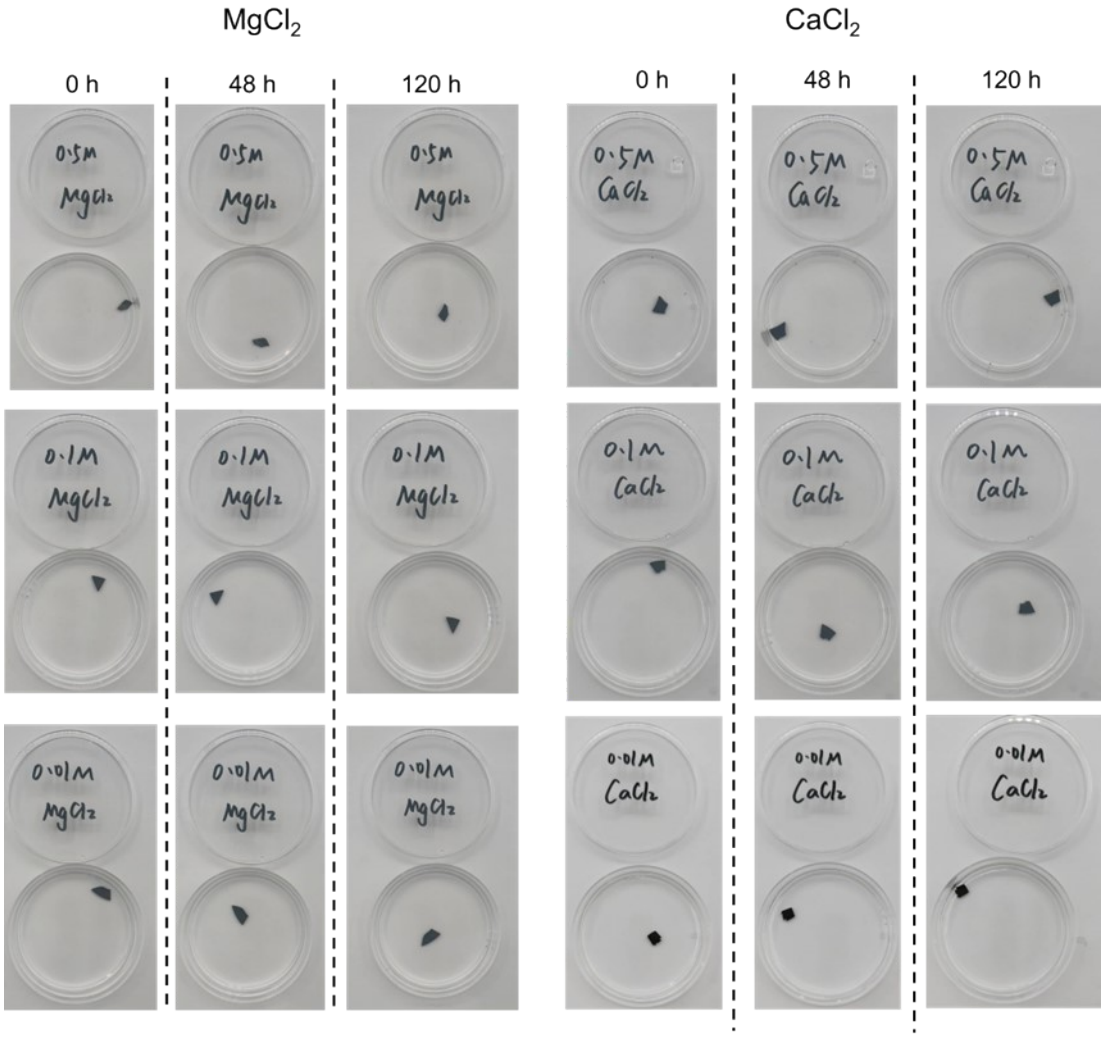

Fig. S24. Photographs of the GO-COF membrane after immersion in different concentration of solutions ($MgCl_2$ and $CaCl_2$) for 0, 48, and 120 h.